

A peer-reviewed version of this preprint was published in PeerJ on 30 March 2017.

[View the peer-reviewed version](https://peerj.com/articles/3133) (peerj.com/articles/3133), which is the preferred citable publication unless you specifically need to cite this preprint.

Odoni DI, Tamayo-Ramos JA, Sloothaak J, van Heck RGA, Martins dos Santos VAP, de Graaff LH, Suarez-Diez M, Schaap PJ. 2017. Comparative proteomics of *Rhizopus delemar* ATCC 20344 unravels the role of amino acid catabolism in fumarate accumulation. PeerJ 5:e3133 <https://doi.org/10.7717/peerj.3133>

Comparative proteomics of *Rhizopus delemar* ATCC 20344 unravels the role of amino acid catabolism in fumarate accumulation

Dorett I Odoni ¹ , Juan A Tamayo-Ramos ¹ , Jasper Sloothaak ¹ , Ruben G A van Heck ¹ , Vitor A P Martins dos Santos ^{1,2} , Leo H de Graaff ¹ , Maria Suarez-Diez ¹ , Peter J Schaap ^{Corresp. 1}

¹ Laboratory of Systems and Synthetic Biology, Wageningen University and Research, Wageningen, The Netherlands

² LifeGlimmer GmbH, Berlin, Germany

Corresponding Author: Peter J Schaap
Email address: peter.schaap@wur.nl

The filamentous fungus *Rhizopus delemar* naturally accumulates relatively high amounts of fumarate. Although the culture conditions that increase fumarate yields are well established, the network underlying the accumulation of fumarate is not yet fully understood. We set out to increase the knowledge about fumarate accumulation in *R. delemar*. To this end, we combined a transcriptomics and proteomics approach to identify key metabolic pathways involved in fumarate production in *R. delemar*, and propose that a substantial part of the fumarate accumulated in *R. delemar* during nitrogen starvation results from the urea cycle due to amino acid catabolism.

1 **Comparative proteomics of *Rhizopus delemar* ATCC 20344**
2 **unravels the role of amino acid catabolism in fumarate**
3 **accumulation**

4 **Dorett I Odoni¹⁺, Juan A Tamayo-Ramos^{1+^}, Jasper Sloothaak¹, Ruben G A van Heck¹,**
5 **Vitor A P Martins dos Santos¹, Leo H de Graaff[†], Maria Suarez-Diez¹ and Peter J**
6 **Schaap¹**

7 ¹ Laboratory of System and Synthetic Biology, Wageningen University and Research,
8 Stippeneng 4, 6708 WE Wageningen, the Netherlands

9 [^] Current address: International Research Centre in Critical Raw Materials-ICCRAM,
10 University of Burgos, Plaza Misael Banuelos s/n, 09001 Burgos, Spain

11
12
13 ⁺Equal contributions

14 [†]Deceased 16 October 2016

15
16 Corresponding author:

17 Peter J Schaap¹

18
19
20 Email address:

21 PJS: peter.schaap@wur.nl

22

23

24 **Abstract**

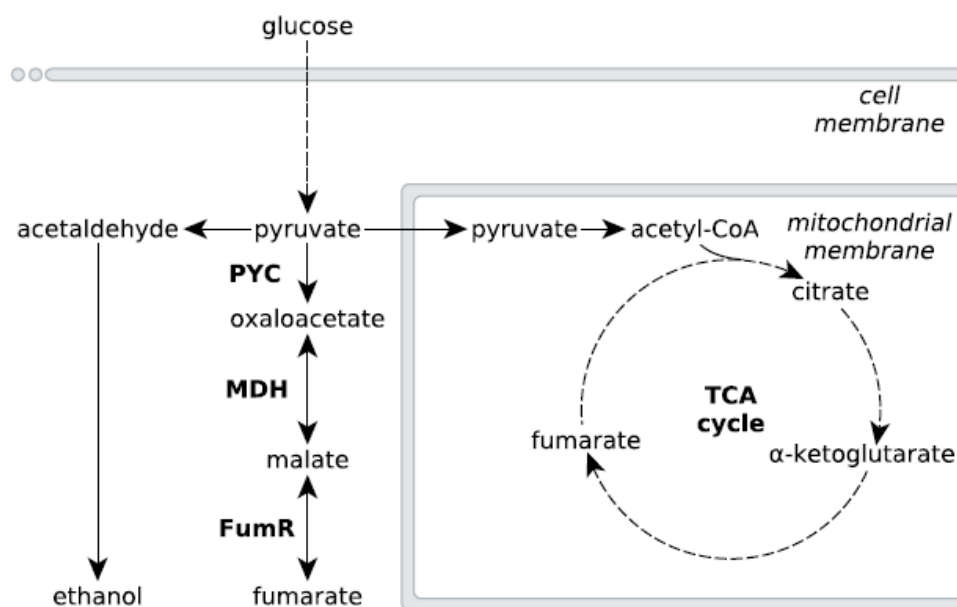
25 The filamentous fungus *Rhizopus delemar* naturally accumulates relatively high amounts of
26 fumarate. Although the culture conditions that increase fumarate yields are well established,
27 the network underlying the accumulation of fumarate is not yet fully understood. We set out
28 to increase the knowledge about fumarate accumulation in *R. delemar*. To this end, we
29 combined a transcriptomics and proteomics approach to identify key metabolic pathways
30 involved in fumarate production in *R. delemar*, and propose that a substantial part of the
31 fumarate accumulated in *R. delemar* during nitrogen starvation results from the urea cycle due
32 to amino acid catabolism.

33

34 **Introduction**

35 Fumarate, a dicarboxylic acid, is an important building block chemical for a number of high-
36 value chemicals and materials. Amongst the microorganisms identified to be natural fumarate
37 producers, the filamentous fungus *Rhizopus delemar* has the highest product yields [1]. The
38 most important factor influencing fumarate production in *R. delemar* is a high carbon:nitrogen
39 ratio; extracellular fumarate accumulation happens after the growth phase, and especially
40 when the nitrogen in the medium has been depleted [2,3]. The choice of nitrogen source has
41 been reported to influence the final fumarate yield [1,4,5], but so far no consensus on these
42 influences has been reached. Another important factor influencing fumarate production in *R.*
43 *delemar* is oxygen availability [1,6]. Under fumarate producing conditions, *R. delemar* forms
44 ethanol and other undesired fermentation by-products [7], directing carbon away from
45 fumarate (Fig. 1). Higher oxygen levels limit the amount of ethanol produced, and thus lead to
46 higher fumarate yields. Fumarate production by fermentation has been extensively reviewed
47 [8,9].

48



49

50 **Figure 1. Metabolic pathways involved in fumarate metabolism in *R. delemar*.**

51 Metabolic flux of *R. delemar* is predominantly directed towards fumarate (under aerobic

52 conditions) or ethanol (under anaerobic conditions). The enzymes of the reductive TCA cycle

53 are indicated in the scheme: PYC = pyruvate carboxylase, MDH = L-malate dehydrogenase

54 and FumR = fumarase.

55

56 Although the culture conditions that increase fumarate accumulation in *R. delemar* are well

57 established, natural product titers still cannot compete with chemical fumarate synthesis. To

58 increase the amount of fumarate produced, *R. delemar* has been genetically modified [10–12],

59 but the occurrence of an ancestral whole-genome duplication as well as more recent gene-

60 duplication events complicate the genetic engineering of *R. delemar* [13]. A more promising

61 approach for biological fumarate production would thus be rewiring the metabolism of a

62 genetically more amenable cell-factory, based on *R. delemar* fumarate synthesis pathways.

63

64 Metabolic engineering approaches to increase fumarate production in microbial cell-factories

65 that do not naturally accumulate high amounts of fumarate would greatly benefit from an in-

66 depth understanding of the underlying metabolic pathways that affect the accumulation of
67 fumarate in the natural fumarate producer *R. delemar*, as well as possible causes for this
68 accumulation. Fumarate can be found as an intermediate in various different metabolic
69 subsystems, and a number of pathways have been investigated for fumarate production in
70 several microbial cell-factories such as *Saccharomyces cerevisiae*, *Torulopsis glabrata*,
71 *Scheffersomyces stipitis* and *Escherichia coli* [14–22]. Despite the large number of pathways
72 leading to fumarate, the current consensus is that the reductive route of the TCA cycle in the
73 cytosol is responsible for fumarate accumulation in *R. delemar* [23–27]. The reductive TCA
74 cycle comprises pyruvate carboxylase (PYC), L-malate dehydrogenase (MDH) and fumarase
75 (FumR), in which pyruvate is consecutively converted to oxaloacetate, L-malate and fumarate
76 (Fig. 1).

77

78 A controversial aspect of this pathway model is FumR. While overexpression of *pyc* and *mdh*
79 gave the expected increase of fumarate in *R. delemar* and *Saccharomyces cerevisiae* [11,20],
80 overexpression of *fumR* in *R. delemar* as well as the introduction of *fumR* in *S. cerevisiae* and
81 *A. niger* was reported to result in more L-malate rather than the accumulation of fumarate
82 [12,20,28]. There has been debate about the role of FumR in fumarate accumulation,
83 discussed by Meussen *et al.* [10]. In summary, the reaction kinetics of FumR favour the
84 conversion of fumarate to L-malate rather than the reverse direction, and FumR activity of
85 acid-producing mycelium is completely blocked in the presence of 2 mM fumarate
86 (unpublished data, cited by [3,10]). This suggests the presence of an alternative pathway that
87 is responsible for fumarate accumulation in *R. delemar*.

88

89 In this study, we aim to provide a holistic overview of the pathways involved in fumarate
90 accumulation in the natural fumarate producer *R. delemar*. To this end, we cultured the *R.*

91 *delemar* strain ATCC 20344 under nitrogen starvation conditions, and varied oxygen
92 availability to induce high (aerobic) and low (anaerobic) fumarate production. Combining
93 transcriptomic and proteomic data obtained from the two conditions, we revealed the
94 relationship between nitrogen metabolism and fumarate accumulation in *R. delemar*, mediated
95 by the urea cycle.

96 **Materials and Methods**

97 **Strains, media and culture conditions**

98 We selected the *R. delemar* strain ATCC 20344 (a kind gift from Adrie J.J. Straathof, Delft
99 University of Technology) to study fumarate production. Note that *R. delemar* is more
100 commonly known as *R. oryzae* (also *Rhizopus nigricans* and *Rhizopus arrhizus*) [29].
101 Depending on the organic acid produced when grown on D-glucose, it is divided into two
102 phylogenetically distinct types: type I strains, which produce primarily L-lactate, and type II
103 strains, which produce mainly fumarate and L-malate [30]. Complete medium agar plates
104 containing 0.3% (w/v) yeast extract, 0.3% (w/v) malt extract, 0.3% (w/v) peptone, 2% (w/v)
105 glycerol, and 2% (w/v) agar were used to generate spores. Mycelial biomass was produced
106 using pre-culture medium containing 1% (w/v) D-glucose, 0.21% (w/v) urea, 0.06% (w/v)
107 KH_2PO_4 , 0.05% (w/v) $\text{MgSO}_4 \cdot 7\text{H}_2\text{O}$ and 0.0018% (w/v) $\text{ZnSO}_4 \cdot 7\text{H}_2\text{O}$. Approximately 10^6
108 spores/mL were inoculated in 1L Erlenmeyer flasks containing 500 mL of pre-culture
109 medium and cultivations were carried out at 35°C and 250 rpm for 24 hours. The mycelium
110 obtained was washed with demineralized water and transferred (≈ 25 g of wet biomass) to
111 production medium, which contained 10% (w/v) D-glucose, 0.06% (w/v) KH_2PO_4 , 0.05%
112 (w/v) $\text{MgSO}_4 \cdot 7\text{H}_2\text{O}$, 0.0018% (w/v) $\text{ZnSO}_4 \cdot 7\text{H}_2\text{O}$, and 1% (w/v) CaCO_3 (used as a
113 neutralizing agent). Batch fermentations were performed at 35°C and 600 rpm in 2.5 L
114 fermentors (Applikon, Schiedam, the Netherlands), with a working volume of 1.75 L.

115 Antifoam 204 was added to each fermentor (85 μ L). The fermentation medium was aerated
116 with 1.0 L/L min, either with filtered air or N₂ gas.

117

118 **Metabolite analysis using HPLC**

119 Extracellular metabolite concentrations were determined by high-performance liquid
120 chromatography (HPLC). A Thermo Accela HPLC, equipped with a Shodex KC-811 column,
121 and coupled to a refractive index detector (Spectrasystem RI-150, sample frequency
122 5.00032Hz) and a UV–VIS detector (Spectrasystem UV1000, λ = 210 nm), was used.
123 Separations were performed by isocratic elution with 0.01 N H₂SO₄ at a flow rate of 0.8
124 mL/min. Crotonic acid (6 mM) was used as an internal standard.

125

126 **RNA isolation and quality control**

127 Frozen mycelium (\approx 100 mg) of *R. delemar* ATCC 20344 was submerged in 1 mL of Trizol
128 reagent in a 2 mL tube, prefilled with a mix of glass beads with the following diameters: 1
129 mm (0.25 g), 0.1 mm (0.37 g), 5 mm (1 bead). Mycelium samples were disrupted using a
130 FastPrep-24 Instrument (MP). After disruption, 200 μ L of chloroform were added and the mix
131 was homogenated for 10 seconds. The mix was poured into phase-lock gel tubes (2 mL), and
132 centrifuged at maximum speed in a table-top centrifuge. The RNA present in the water phase
133 was purified using the RNeasy Mini Kit (Qiagen), following the manufacturer's instructions.
134 RNA integrity was assessed with an Experion system (Bio-Rad), and only high quality
135 samples (RIN value \geq 8) were selected for whole transcriptome shotgun sequencing.

136

137 **RNA sequencing and quality check**

138 Illumina RNA sequencing (RNA seq) using the Casava pipeline version 1.8.2 and subsequent
139 quality analysis of the FASTQ sequence reads was performed by BaseClear (Leiden, the

140 Netherlands). The number of reads obtained was 20'539'199 for the aerobic and 24'519'028
141 for the anaerobic condition, with an average quality score (Phred) of 37.59 and 37.91,
142 respectively. The raw data has been submitted to the EMBL-EBI database, and can be found
143 under the accession number PRJEB14210.

144

145 **RNA seq data processing**

146 The RNA seq reads were filtered using SortMeRNA v1.9 [31], cutadapt v1.2.1 [32] and
147 PRINSEQ v0.20.2 [33]. *De novo* assembly of the reads that passed the quality filtering was
148 performed using the IDBA-UD assembler v1.1 [34]. Read mapping and transcript coverage
149 calculations were performed using Bowtie2 v 2.2.2 [35] and BEDTools [36]. Note that in
150 contrast to the proteomics analysis, which was performed on both biological replicates, only
151 one biological replicate per condition was sent for RNA sequencing. The average nucleotide
152 coverage is thus an indication of the transcript levels of a given transcript the time of
153 sampling, not the average of two biological replicates.

154

155 **Preparation of cell free extracts for proteomic analysis**

156 *R. delemar* ATCC 20344 mycelium samples (2-3 g, press-dried), were washed with an ice-
157 cold 20 mM HEPES buffer pH 7.6, containing 150 mM NaCl, and resuspended in the same
158 solution containing 1% (v/v) protease inhibitor cocktail for yeast and fungi (Sigma).
159 Mycelium suspensions were immediately disrupted using a French press (8000 psi). Cell free
160 extracts were centrifuged for 5 min at low speed (500 g), in order to remove unbroken cells
161 and pellet debris. The remaining supernatants were further processed for LC-MS/MS
162 analysis.

163

164 **Sample preparation for LC-MS/MS**

165 The protein content of the *R. delemar* ATCC 20344 cell free extracts was determined using
166 the BCA protein assay (Thermo Fisher). Membrane-bound proteins were solubilised by
167 mixing volumes of each sample, containing 25 µg of protein, with equal volumes of a 2x
168 solution of 20 mM HEPES pH 7.6, containing 1 M 6-aminocaproic acid and 10 g L⁻¹ of n-
169 dodecyl-beta-D-maltoside. Cell free extract-detergent mixes were incubated in a thermoblock
170 for 1 h at 20°C and vigorous stirring (1000 rpm). Afterwards, samples were sonicated in a
171 water bath for 15 min, and finally they were centrifuged at 22000 g, in a benchtop centrifuge,
172 for 30 min. Obtained supernatants were subsequently concentrated using MMicrocon YM-10
173 columns (cutoff, 10 kDa; Millipore, Eschborn, Germany).

174

175 Samples from each biological replicate and culture condition were loaded into a 12% SDS-
176 polyacrylamide gel, which was run until the loaded samples entered the gel. The gel was
177 stained according to the manufacturer's instructions using Page Blue staining (Fermentas) and
178 rinsed with ultrapure water. Each sample-gel lane was cut into one slice (approx. 1 cm²),
179 carefully sliced into smaller pieces of about 1 mm³ and transferred into microcentrifuge tubes.
180 Samples were destained and equilibrated through three washing steps using the following
181 solutions: 50 mM ammonium bicarbonate (ABC) (incubated 5 min), ABC/acetonitrile (1:1,
182 v/v) (incubated 5 min) and neat acetonitrile (incubated 5 min). These washing steps were
183 repeated two times. The gel samples were then swelled in 10 mM dithiothreitol (DTT) for 20
184 min at 56°C to reduce protein disulfide bonds. Subsequently, the DTT solutions were
185 removed and samples were alkylated with 50 mM 2-chloroacetamide in ABC, for 20 min, at
186 room temperature, in the dark. The 2-chloroacetamide solutions were removed, and samples
187 were again washed twice with: neat acetonitrile (incubated 5 min), ABC (incubated 5 min)
188 and neat acetonitrile (incubated 5 min). Approximately 150 µL of digestion buffer, containing
189 sequencing grade modified trypsin (12.5 ng/µL) (Promega) in ABC, was added to each

190 sample, making sure that all gel pieces were kept wet during digestion (adding, if necessary,
191 additional ABC solution). Protein samples were digested overnight at 37°C. Peptide digestion
192 products were extracted by adding 50 µL of 2% trifluoroacetic acid (TFA), followed by an
193 incubation step in a thermoblock for 20 min, at room temperature and vigorous stirring (1400
194 rpm). Gel pieces were then subjected to 20 s sonication in a water bath, centrifuged and
195 supernatants were transferred to new tubes. The peptide extraction step was then repeated
196 once by washing the gel pieces with buffer B (80% acetonitrile, 0.1% formic acid) followed
197 by the mentioned incubation and sonication steps. Supernatants from both extractions were
198 pooled and samples were placed in a vacuum centrifuge for acetonitrile evaporation until 20-40
199 µL were left. Finally, samples were acidified by addition of TFA (1:1, v/v) and peptide clean-
200 up procedure, prior to LC-MS/MS analysis, was performed using the “STop And Go
201 Extraction” procedure as described before [37].

202

203 **Mass spectrometric measurements and proteomic data analysis**

204 LC-MS/MS analysis was performed at the Radboud Proteomics Centre as described
205 previously [38]. Measurements were performed by nanoflow reversed-phase C18 liquid
206 chromatography (EASY nLC, Thermo Scientific) coupled online to a 7 Tesla linear ion trap
207 Fourier-Transform ion cyclotron resonance mass spectrometer (LTQ FT Ultra, Thermo
208 Scientific). The LC-MS/MS spectra obtained were identified and quantified using the
209 maxQuant software [39]. The peptides were mapped against the *in silico* proteomes of *R.*
210 *delemar* ATCC 20344 (obtained from the transcriptomics experiment) and RA 99-880
211 (obtained from Genbank, Project ID: 13066 [13]) with the default settings, described in [40].
212 Only proteins with 2 or more unique peptide hits were considered for further analysis. The
213 mass spectrometry proteomics data have been deposited to the ProteomeXchange Consortium
214 via the PRIDE [41] partner repository with the dataset identifier PXD004600.

215

216 **Metabolic pathway enrichment analysis**

217 Metabolic enzymes were annotated using PRIAM [42], and subsequently assigned to KEGG
218 pathways [43,44]. Enrichment analysis of differentially expressed pathways was performed
219 using the hypergeometric test implementation (“phyper”) of the R software environment [45].
220 We used the identified proteins that could be mapped to a KEGG pathway as the universe
221 (with size $N = 277$). Note that the terms “differentially expressed” and “overexpressed” refer
222 to differences in relative protein abundances, and denote a fold-change of 1.5 and 2 as lenient
223 and stringent thresholds.

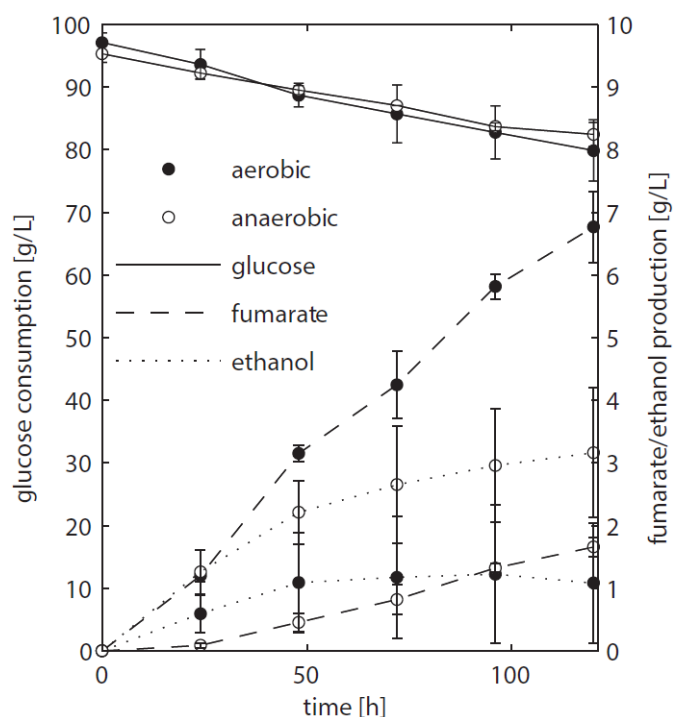
224

225 **Results and Discussion**

226 **Fumarate and ethanol production of ATCC 20344 grown under aerobic and anaerobic** 227 **conditions**

228 We chose to work with *R. delemar* ATCC 20344, henceforth referred to as ATCC 20344, for
229 its ability to produce fumarate in high quantities [46]. ATCC 20344 was grown in batch
230 fermentations under nitrogen starved conditions. The fumarate production rate was controlled
231 by either supplying filtered air to the culture medium (aerobic condition), or restricting the
232 amount of oxygen by flushing the system with N_2 (anaerobic condition). D-glucose, fumarate
233 and ethanol concentrations in the supernatant were measured *via* High Performance Liquid
234 Chromatography (HPLC) to determine the time point with the largest difference in fumarate
235 yield. The HPLC analysis showed comparable D-glucose consumption rates in the two
236 conditions (Fig. 2), with an average of 0.15 ± 0.03 g/h and 0.11 ± 0.03 g/h for the aerobic and
237 anaerobic condition, respectively. Fumarate production was higher in the aerobic condition,
238 whereas in the anaerobic condition ethanol production prevailed. Note that Lin *et al.* showed
239 that *Rhizopus spp.* grow very poorly under absolute anaerobic conditions, but that most of the
240 tested strains grew “quite well” under microaerobic conditions [47]. The use of silicone

241 tubing on our fermentors, which are slightly oxygen permeable even when flushed with pure
 242 nitrogen gas [48], allowed ATCC 20344 to grow at a normal rate, while keeping fumarate
 243 production to a minimum. However, the amount of oxygen entering through the silicone
 244 tubing was below the detection limit of the probes measuring dissolved oxygen in the
 245 fermentors, and we refer to the two conditions as “aerobic” and “anaerobic” rather than
 246 “aerobic” and “microaerobic”.
 247



248

249 **Figure 2. HPLC analysis of fermentation broth of *R. delemar* ATCC 20344 grown under**
 250 **aerobic and anaerobic conditions.**

251 Total D-glucose consumption and fumarate and ethanol production of *R. delemar* ATCC

252 20344. The measurement points show the average of two biological replicates.

253

254 The fumarate yields (gram per gram substrate D-glucose consumed) are summarised in Table

255 1. The maximum fumarate yield (0.41 ± 0.06 g/g) in the aerobic condition was observed after

256 96 hours of fermentation. A comparable yield (0.35 ± 0.05 g/g) was already observed after 24

257 hours of fermentation. In contrast, the fumarate yield in the anaerobic condition increased
 258 continuously at a slow pace, being highest after 120 hours of fermentation (0.13 ± 0.02 g/g).
 259 Thus, the largest difference in fumarate yield between the two conditions was observed at the
 260 start of the experiment, and we chose $t = 24$ h as the time point for the transcriptome and
 261 proteome analyses.
 262

263 **Table 1. Fumarate yields of ATCC 20344 grown under aerobic and anaerobic**
 264 **conditions.**

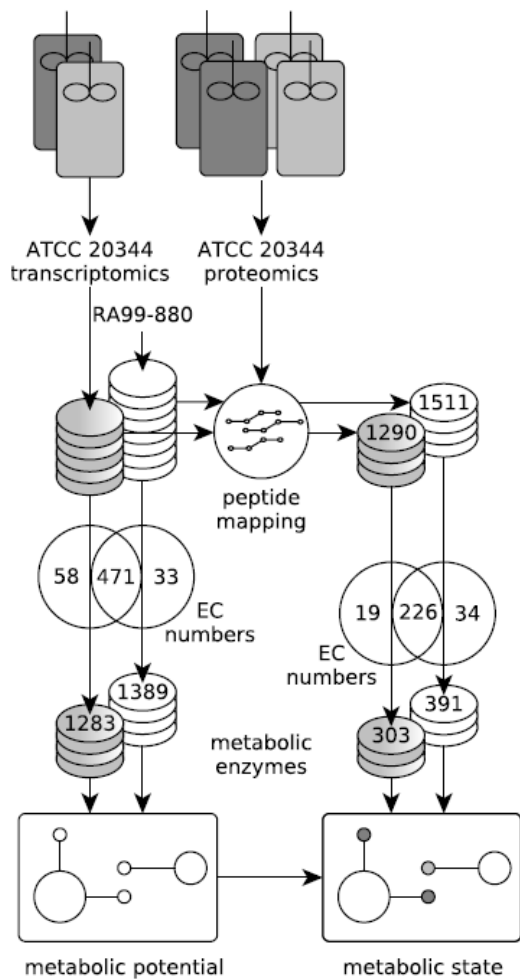
Time [h]	Fumarate yield \pm sd [g/g D-glucose]	
	aerobic	anaerobic
24	0.349 ± 0.055	0.029 ± 0.015
48	0.375 ± 0.001	0.077 ± 0.015
72	0.380 ± 0.055	0.098 ± 0.012
96	0.411 ± 0.063	0.115 ± 0.014
120	0.397 ± 0.044	0.132 ± 0.022

265

266 **Transcriptome and proteome of ATCC 20344 under high and low fumarate producing**
 267 **conditions**

268 Enzyme activities, and thus metabolism, are affected by various factors such as post-
 269 translational modifications, allosteric control, and substrate availability. Metabolic fluxes can
 270 therefore not be inferred directly from protein abundances. Nevertheless, contrasting enzyme
 271 abundance levels between the high and low fumarate producing condition (ATCC 20344
 272 snapshot proteomes) indicate differences in the metabolic state of ATCC 20344 at the time
 273 point of sampling. To determine differential protein abundances *via* LC-MS/MS, a reference
 274 proteome database is required for peptide mass fingerprinting. To date, *R. delemar* RA 99-
 275 880, henceforth referred to as RA 99-880, is the only fully sequenced *R. delemar* strain of

276 which also the proteome is publicly available [13]. However, if the RA 99-880 reference
277 proteome is used as only reference database, conservative amino acid substitutions in ATCC
278 20344 will reduce the sensitivity, as protein identification relies on an exact peptide mass. To
279 provide a complete database of the metabolic potential as well as an overview of the
280 metabolic state of ATCC 20344 under high and low fumarate producing conditions, we
281 combined transcriptomic and proteomic data of ATCC 20344 grown under high and low
282 fumarate producing conditions. The transcriptome was used to construct a database of the
283 ATCC 20344 *in silico* proteome, and the relative protein abundances were obtained by
284 mapping the peptides from the snapshot proteomes against both the ATCC 20344 and RA 99-
285 880 *in silico* proteomes, the latter to account for possible errors in the *de novo* transcript
286 assembly. The experimental setup is outlined in Fig. 3.
287



288

289 **Figure 3. Experimental setup.**

290 Workflow to establish the metabolic potential and metabolic state of ATCC 20344 grown
 291 under high and low fumarate producing conditions. The metabolic enzymes predicted in the
 292 ATCC 20344 and RA 99-880 *in silico* proteomes provide a map of the metabolic potential,
 293 while the metabolic enzymes identified in the proteomics experiment were used to determine
 294 the metabolic state of ATCC 20344 under high and low fumarate producing conditions.

295

296 The RNA seq reads obtained from the aerobic and anaerobic conditions were combined into
 297 one dataset, and assembled *de novo*, resulting in 13'531 contigs (File S1). EC numbers were
 298 assigned to the six-frame translation products of the *de novo* contigs, as well as to the RA 99-
 299 880 reference proteome (File S2). In ATCC 20344, we predicted 1283 metabolic enzymes,

300 covering 529 EC numbers. In RA 99-880, we predicted 1389 metabolic enzymes, covering
 301 504 EC numbers. The metabolic enzymes were mapped to KEGG pathway maps [43,44] in
 302 order to obtain a rough estimate of the metabolic potential of *R. delemar*.

303

304 The proteins obtained from the aerobic and anaerobic conditions were subjected to a shotgun
 305 proteomics analysis. A total of 1290 and 1511 proteins were identified in the ATCC 20344
 306 and RA 99-880 proteomes, respectively. Roughly one third of the identified proteins
 307 comprised metabolic enzymes. A list of all EC numbers predicted in the ATCC 20344 and
 308 RA 99-880 *in silico* proteomes, as well as the relative protein abundances and average
 309 nucleotide coverages of the proteins and transcripts identified in the experimental conditions,
 310 can be found in Table S3. The protein pathway coverage (number of ECs per pathway
 311 covered by proteins with the predicted function in ATCC 20344 and RA 99-880) is given in
 312 Table S4.

313

314 **Metabolic pathway enrichment analysis**

315 To determine which pathways play an important role in fumarate accumulation in ATCC
 316 20344, we obtained a list of enzymatic proteins that directly consume or produce fumarate
 317 according to the KEGG database [43,44], and analysed their presence and abundance in the
 318 ATCC 20344 high and low fumarate producing conditions (Table 2). In addition, we
 319 performed pathway enrichment analysis of differentially expressed enzymes (Table 3, Table
 320 S4).

321 **Table 2. List of enzymes involved in fumarate metabolism with their respective protein**
 322 **abundances under high and low fumarate producing conditions.**

EC number	Consensus protein identifier ^a	Relative protein abundance \pm sd [%]		Log ₂ FC aerobic/anaerobic	Enzyme name
		aerobic	anaerobic		

4.2.1.2	Rd_01690	1.51 ± 0.16	0.66 ± 0.06	1.21	fumarate hydratase (fumarase, FumR)
4.3.2.1	Rd_00962	0.09 ± 0.01	0.06 ± 0.02	0.60	argininosuccinate lyase (ASL)
1.3.98.1	Rd_00873	0.04 ± 4e-3	0.01 ± 2e-3	1.34	dihydroorotate dehydrogenase
3.7.1.2	Rd_01207	0.03 ± 3e-3	0.00	-	fumarylacetoacetase
1.3.5.1	Rd_01783	0.01 ± 2e-3	0.00	-	succinate dehydrogenase
4.3.2.2	Rd_00964	5e-3 ± 7e-4	0.01 ± 8e-7	-1.59	adenylosuccinate lyase

323 ^aIdentifiers refer to IDs in Table S3. Note that, where possible, ATCC 20344 enzymes were
324 prioritised. In this case, all enzymes were identified in the ATCC 20344 proteome.

325

326 **Table 3. Metabolic pathway enrichment analysis.**

Pathway	# ECs in reference pathway	# proteins (ECs) identified	Differentially expressed		Overexpressed (aerobic)			
			# proteins (1.5-fold)	p-value	# proteins (1.5-fold)	p-value	# proteins (2-fold)	p-value
Alanine, aspartate and glutamate metabolism	50	16 (12)	15	0.040	10	0.102	7	0.264
Arginine biosynthesis	32	14 (12)	13	0.070	10	0.033	5	0.534
beta-Alanine metabolism	37	11 (8)	9	0.389	9	0.011	9	0.001
Citrate cycle (TCA cycle)	25	19 (15)	14	0.589	10	0.292	9	0.143
Glycolysis / Gluconeogenesis	49	31 (19)	19	0.957	10	0.946	9	0.777
Oxidative phosphorylation	11	20 (8)	16	0.327	14	0.014	9	0.189
Pyrimidine	65	13 (11)	11	0.267	9	0.056	6	0.243

metabolism								
Pyruvate metabolism	68	23 (15)	17	0.565	11	0.433	11	0.102
Valine, leucine and isoleucine degradation	38	14 (10)	11	0.446	8	0.230	8	0.055

327

328 We found that, amongst the enzymes which interact directly with fumarate and were
329 identified in the ATCC 20344 snapshot proteomes, FumR (EC 4.2.1.2), is the most highly
330 abundant enzyme, both under high and low fumarate producing conditions (Table 2).

331 Although there is no clear enrichment of the TCA cycle enzymes among the differentially
332 expressed metabolic proteins (Table 3), the three enzymes of the reductive TCA cycle, PYC
333 (EC 6.4.1.1), MDH (EC 1.1.1.37), and FumR (EC 4.2.1.2), are all overexpressed in the high
334 fumarate producing condition (Table S3).

335

336 The second most highly abundant protein related to fumarate metabolism is argininosuccinate
337 lyase (ASL) (EC 4.3.2.1). ASL is a urea cycle enzyme involved in arginine biosynthesis. The
338 arginine biosynthesis pathway showed a significant number of differentially expressed
339 proteins (Table 3), and we found that the enzymes comprising the urea cycle are
340 overexpressed in the high fumarate producing condition (Table 4). This suggests that in
341 ATCC 20344, the urea cycle plays an important role in fumarate accumulation. Most
342 interestingly, ASL and FUM constitute a crucial link between carbon and nitrogen
343 metabolism by connecting the TCA- and urea cycles (also referred to as “Krebs bicycle”).

344

345
346

Table 4. Urea cycle enzymes with their respective protein abundances under high and low fumarate producing conditions.

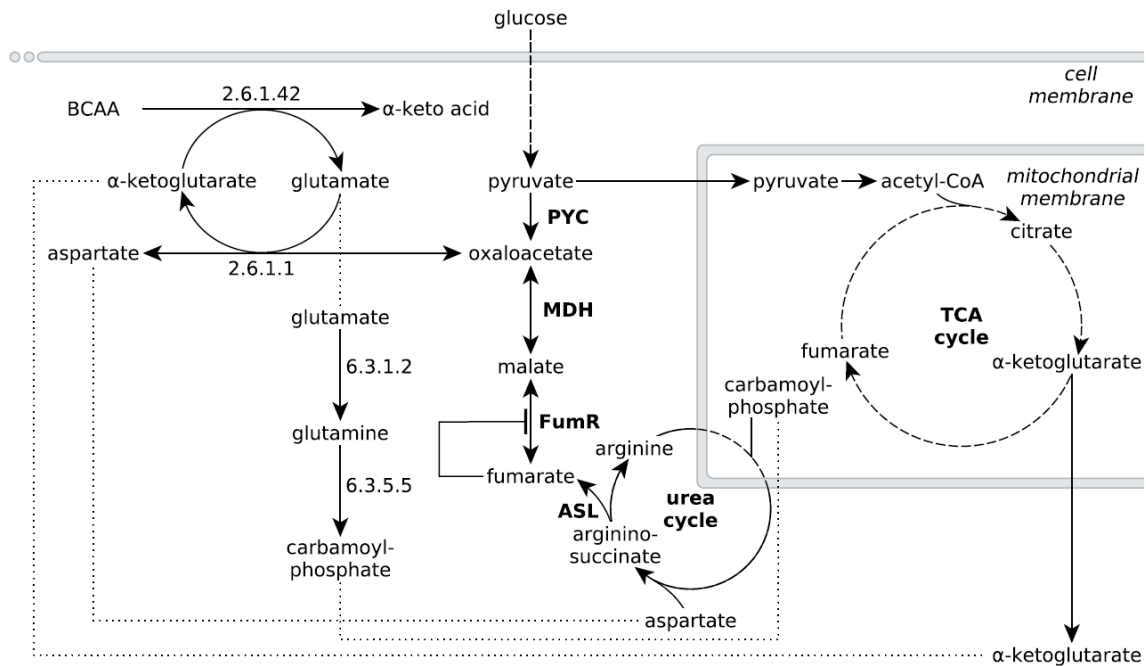
EC number	Consensus protein identifier ^a (ref)	Relative protein abundance \pm sd [%]		Log ₂ FC aerobic/anaerobic	Enzyme name
		aerobic	anaerobic		
2.1.3.3	Rd_01058 (A)	0.03 \pm 0.01	0.02 \pm 8e-3	0.51	ornithine carbamoyltransferase (OTC)
6.3.4.5	Rd_01708 (R)	0.86 \pm 0.07	0.57 \pm 0.05	0.59	argininosuccinate synthase (ASS)
6.3.4.5	Rd_01709 (R)	0.00	0.04 \pm 0.02	-	argininosuccinate synthase (ASS)
4.3.2.1	Rd_00962 (A)	0.09 \pm 0.01	0.06 \pm 0.02	0.60	argininosuccinate lyase (ASL)
3.5.3.1	Rd_00988 (R)	0.13 \pm 0.02	0.07 \pm 0.01	0.97	arginase (ARG)
3.5.3.1	Rd_00989 (R)	0.19 \pm 0.02	0.11 \pm 0.03	0.76	arginase (ARG)

347 ^aIdentifiers refer to IDs in Table S3. Note that, where possible, ATCC 20344 enzymes were
348 prioritised. Letters in brackets refer to the reference proteome, with A = ATCC 20344 and R =
349 RA 99-880.

350

351 The observed protein abundances for FumR and ASL offer an explanation for the importance
352 of a high carbon:nitrogen ratio for fumarate accumulation in *Rhizopus spp.* In humans,
353 starvation induces a net breakdown of stored energy sources, starting with fatty acids and,
354 when exposed to prolonged starving conditions, proteins from muscle tissue. The degradation
355 of protein, or amino acids, results in the liberation of ammonia, which is then carried to the
356 urea cycle as L-glutamate. In the urea cycle, the L-glutamate is converted to urea, which is
357 subsequently excreted. Based on the significant enrichment scores of pathways involved in

358 amino acid metabolism (Table 3), we propose that the nitrogen starvation, induced by the
 359 transfer of ATCC 20344 from growth- to production medium, triggers a similar switch in
 360 metabolism, and amino acid catabolism starts to occur. The resulting fluxes through the urea
 361 cycle yield an excess of fumarate (Fig. 4).
 362



363

364 **Figure 4. Extended network of metabolic pathways involved in fumarate metabolism in**
 365 ***R. delemar*.**

366 The extended model of fumarate accumulation reconstructed from the ATCC 20344 snapshot
 367 proteomes under high and low fumarate producing conditions takes the formation of fumarate
 368 *via* the urea cycle into account.

369

370 Specifically, the pathway for the degradation of the branched-chain amino acids (BCAA)
 371 valine, leucine and isoleucine shows a significant number of overexpressed enzymes in high
 372 fumarate producing condition. BCAA catabolism is initiated by BCAA aminotransferase (EC
 373 2.6.1.42), which catalyses the transfer of an amino group from any of the three BCAAs to α -
 374 ketoglutarate, yielding L-glutamate and the respective α -keto acid as products (Fig. 4). Under

375 starvation conditions in which both the nitrogen and carbon source in the culture medium are
376 limited, the carbon skeletons of the deaminated amino acids can be used to replenish acetyl-
377 CoA (from leucine), or the TCA cycle intermediate succinyl-CoA (from valine) or both of
378 these metabolites (from isoleucine), and thereby, ultimately, to generate energy for growth.
379 Under conditions of excess carbon and limited nitrogen, however, it is unlikely that amino
380 acid catabolism is driven by energy demand of the organism. More importantly, it is crucial
381 for *R. delemar* grown under nitrogen depleted conditions to decouple carbon catabolism from
382 cell proliferation, as there is little nitrogen available for *de novo* protein biosynthesis.

383

384 One way to decouple carbon catabolism from biomass formation is by reducing the amount of
385 ATP generated. Under aerobic growth conditions, ATP is generated *via* oxidative
386 phosphorylation. Under anaerobic conditions, *R. delemar* generates ATP *via* ethanol
387 fermentation (Fig. 1). Another option for ATP generation is alternative respiration, mediated
388 by the key enzyme alternative oxidase (AOX). AOX diverts the electrons passing through the
389 electron transport chain in the mitochondria at the ubiquinone pool and transfers them directly
390 to oxygen, thereby bypassing the oxidative phosphorylation complexes III and IV, resulting in
391 an overall lower ATP yield. Gu *et al.* found that the activity of AOX is positively correlated
392 with fumarate production in *R. delemar* [49]. In contrast, we identified AOX (Rd_00967 (A))
393 only in the snapshot proteome of the anaerobic condition. The transcriptomics measurements
394 further underpin our proteomics results, since *aox* was overexpressed (> 4-fold) in the
395 anaerobic condition (Table S3). This might seem counterintuitive at first, since the expression
396 of *aox* is generally regarded as a means of dealing with increased oxidative stress. However,
397 the electron flow through AOX has been found to be inversely proportional to nitrogen
398 availability in various different plant systems [50]. The increase of AOX under nitrogen
399 limited conditions and the resulting decrease of the respiratory ATP yield have been

400 associated with a deliberately reduced efficiency in converting carbon to biomass; by using
401 the non-energy conserving AOX, the “redundant” carbohydrate can be metabolised without
402 being coupled to growth.

403

404 Another way of decoupling carbon catabolism from energy generation, and thereby cell
405 proliferation, is channelling the products from amino acid degradation to the mitochondria for
406 mitochondrial protein synthesis, and thereby away from cytosolic protein synthesis; a
407 mechanism suggested to take place under nitrogen starvation conditions in human cells,
408 irrespective of the D-glucose availability [51]. In this, amino acid catabolism is the first step
409 to adapt to nitrogen limiting conditions, and we propose that, in a similar mechanism, the urea
410 cycle plays a key role for the accumulation of fumarate in *R. delemar*. This is supported by
411 the work of Chen *et al.*, who showed that, from a range of selected enzymes, overexpressing
412 ASL, while keeping the expression of adenylosuccinate lyase low, resulted in the highest
413 fumarate titer in *Torulopsis glabrata* [14].

414

415 **Conclusions**

416 The accumulation of fumarate in the natural fumarate producer *R. delemar* has been mostly
417 attributed to the consecutive conversion of pyruvate to oxaloacetate, L-malate and fumarate
418 by cytosolic enzymes of the reductive TCA cycle. In addition, our proteomics data have
419 revealed that the nitrogen-limitation under fumarate producing conditions induces amino acid
420 catabolism, which leads to an increased flux through the urea cycle. Our comparative
421 proteomics analysis of high and low fumarate producing conditions in *R. delemar* ATCC
422 20344 has thus resulted in a novel holistic view on fumarate production that expands the
423 knowledge on fumarate production in this fungus.

424

Acknowledgements

We would like to thank Sybe Hartmans, Michael Volpers and Brendan Ryback for critically reading and commenting on draft versions of the manuscript. In addition, we would like to thank Bastian Hornung for valuable input for the RNA seq data analysis, Ruud Weusthuis for valuable feedback on general aspects of this manuscript, and Tom Schonewille and Merlijn van Gaal for their contribution in the experimental part of this work.

References

1. Foster JW, Waksman SA. The Production of Fumaric Acid by Molds Belonging to the Genus *Rhizopus*. *J Am Chem Soc. American Chemical Society*; 1939;61: 127–135.
2. Magnuson J, Lasure L. Organic acid production by filamentous fungi. *Adv fungal Biotechnol Ind Agric Med*. 2004; 307–340.
3. Goldberg I, Rokem JS, Pines O. Organic acids: old metabolites, new themes. *J Chem Technol Biotechnol*. 2006;81: 1601–1611.
4. Rhodes R a, Moyer a J, Smith ML, Kelley SE. Production of fumaric acid by *Rhizopus arrhizus*. *Appl Microbiol*. 1959;7: 74–80.
5. Z.Y. Zhang, B. Jin JMK. Production of lactic acid and byproducts from waste potato starch by *Rhizopus arrhizus* : role of nitrogen sources. *World J Microbiol Biotechnol*. 2007;23: 229–236.
6. J. W. Foster, S.F. Carson, D.S Anthony, J.B. Davis, W.E. Jefferson MVL. Aerobic formation of fumaric acid in the mold *Rhizopus nigricans*: Synthesis by direct C2 condensation. *Proc Natl Acad Sci*. 1949;35.
7. Wright BE, Longacre A, Reimers J. Models of metabolism in *Rhizopus oryzae*. *J Theor Biol*. 1996;182: 453–7.
8. Straathof AJJ, van Gulik WM. Production of fumaric acid by fermentation. *Subcell Biochem*. 2012;64: 225–40.
9. Roa Engel CA, Straathof AJJ, Zijlmans TW, van Gulik WM, van der Wielen LAM. Fumaric acid production by fermentation. *Appl Microbiol Biotechnol*. 2008;78: 379–89.
10. Meussen BJ, de Graaff LH, Sanders JPM, Weusthuis RA. Metabolic engineering of *Rhizopus oryzae* for the production of platform chemicals. *Appl Microbiol Biotechnol*. 2012;94: 875–86.
11. Zhang B, Skory CD, Yang S-T. Metabolic engineering of *Rhizopus oryzae*: effects of overexpressing *pyc* and *pepc* genes on fumaric acid biosynthesis from glucose. *Metab Eng*. 2012;14: 512–20.
12. Zhang B, Yang S-T. Metabolic engineering of *Rhizopus oryzae*: Effects of overexpressing *fumR* gene on cell growth and fumaric acid biosynthesis from glucose. *Process Biochem*. 2012;47: 2159–2165.
13. Ma L-J, Ibrahim AS, Skory C, Grabherr MG, Burger G, Butler M, et al. Genomic analysis of the basal lineage fungus *Rhizopus oryzae* reveals a whole-genome duplication. *PLoS Genet*. 2009;5: e1000549.
14. Chen X, Wu J, Song W, Zhang L, Wang H, Liu L. Fumaric acid production by *Torulopsis glabrata*: engineering the urea cycle and the purine nucleotide cycle. *Biotechnol Bioeng*. 2015;112: 156–67.

- 468 15. Li N, Zhang B, Wang Z, Tang Y-J, Chen T, Zhao X. Engineering *Escherichia coli* for
469 fumaric acid production from glycerol. *Bioresour Technol.* 2014;174: 81–7.
- 470 16. Song CW, Kim DI, Choi S, Jang JW, Lee SY. Metabolic engineering of *Escherichia*
471 *coli* for the production of fumaric acid. *Biotechnol Bioeng.* 2013;110: 2025–34.
- 472 17. Wei L, Liu J, Qi H, Wen J. Engineering *Scheffersomyces stipitis* for fumaric acid
473 production from xylose. *Bioresour Technol.* 2015;187: 246–54.
- 474 18. Xu G, Chen X, Liu L, Jiang L. Fumaric acid production in *Saccharomyces cerevisiae*
475 by simultaneous use of oxidative and reductive routes. *Bioresour Technol.* 2013;148:
476 91–6.
- 477 19. Xu G, Liu L, Chen J. Reconstruction of cytosolic fumaric acid biosynthetic pathways
478 in *Saccharomyces cerevisiae*. *Microb Cell Fact.* BioMed Central; 2012;11: 24.
- 479 20. Xu G, Zou W, Chen X, Xu N, Liu L, Chen J. Fumaric acid production in
480 *Saccharomyces cerevisiae* by *in silico* aided metabolic engineering. *PLoS One.* Public
481 Library of Science; 2012;7: e52086.
- 482 21. Zhang T, Wang Z, Deng L, Tan T, Wang F, Yan Y. Pull-in urea cycle for the
483 production of fumaric acid in *Escherichia coli*. *Appl Microbiol Biotechnol.* 2015;99:
484 5033–44.
- 485 22. Chen X, Zhu P, Liu L. Modular optimization of multi-gene pathways for fumarate
486 production. *Metab Eng.* 2016;33: 76–85.
- 487 23. Romano AH, Bright MM, Scott WE. Mechanism of fumaric acid accumulation in
488 *Rhizopus nigricans*. *J Bacteriol.* 1967;93: 600–4.
- 489 24. Overman SA, Roman H. Pyruvate carboxylase of *Rhizopus nigricans* and its role in
490 fumaric acid production. *Biochem Biophys Res Commun.* 1969;37: 457–463.
- 491 25. Osmani S A, Scrutton MC. The sub-cellular localisation and regulatory properties of
492 pyruvate carboxylase from *Rhizopus arrhizus*. *Eur J Biochem.* 1985;147: 119–28.
- 493 26. Kenealy W, Zaady E, du Preez JC, Stieglitz B, Goldberg I. Biochemical Aspects of
494 Fumaric Acid Accumulation by *Rhizopus arrhizus*. *Appl Environ Microbiol.* 1986;52:
495 128–33.
- 496 27. Peleg Y, Battat E, Scrutton M, Goldberg I. Isoenzyme pattern and subcellular
497 localisation of enzymes involved in fumaric acid accumulation by *Rhizopus oryzae*.
498 *Appl Microbiol Biotechnol.* Springer-Verlag; 1989;32: 334–339.
- 499 28. de Jongh WA, Nielsen J. Enhanced citrate production through gene insertion in
500 *Aspergillus niger*. *Metab Eng.* 2008;10: 87–96.
- 501 29. Abe A, Oda Y, Asano K, Sone T. *Rhizopus delemar* is the proper name for *Rhizopus*
502 *oryzae* fumaric-malic acid producers. *Mycologia.* 2007;99: 714–22.
- 503 30. Abe A, Sone T, Sujaya IN, Saito K, Oda Y, Asano K, et al. rDNA ITS sequence of
504 *Rhizopus oryzae*: its application to classification and identification of lactic acid
505 producers. *Biosci Biotechnol Biochem.* Japan Society for Bioscience, Biotechnology,
506 and Agrochemistry; 2003;67: 1725–31.
- 507 31. Kopylova E, Noé L, Touzet H. SortMeRNA: fast and accurate filtering of ribosomal
508 RNAs in metatranscriptomic data. *Bioinformatics.* 2012;28: 3211–7.
- 509 32. Martin M. Cutadapt removes adapter sequences from high-throughput sequencing
510 reads. *EMBnet.journal.* 2011. pp. 10–12.
- 511 33. Schmieder R, Edwards R. Quality control and preprocessing of metagenomic datasets.
512 *Bioinformatics.* 2011;27: 863–4.
- 513 34. Peng Y, Leung HCM, Yiu SM, Chin FYL. IDBA-UD: a *de novo* assembler for single-
514 cell and metagenomic sequencing data with highly uneven depth. *Bioinformatics.*
515 2012;28: 1420–8.
- 516 35. Langmead B, Salzberg SL. Fast gapped-read alignment with Bowtie 2. *Nat Methods.*
517 2012;9: 357–9.

- 518 36. Quinlan AR, Hall IM. BEDTools: a flexible suite of utilities for comparing genomic
519 features. *Bioinformatics*. 2010;26: 841–2.
- 520 37. Rappsilber J, Ishihama Y, Mann M. Stop and Go Extraction Tips for Matrix-Assisted
521 Laser Desorption/Ionization, Nanoelectrospray, and LC/MS Sample Pretreatment in
522 Proteomics. *Anal Chem*. American Chemical Society; 2003;75: 663–670.
- 523 38. Rajala N, Hensen F, Wessels HJCT, Ives D, Gloerich J, Spelbrink JN. Whole cell
524 formaldehyde cross-linking simplifies purification of mitochondrial nucleoids and
525 associated proteins involved in mitochondrial gene expression. *PLoS One*. Public
526 Library of Science; 2015;10: e0116726.
- 527 39. Cox J, Mann M. MaxQuant enables high peptide identification rates, individualized
528 p.p.b.-range mass accuracies and proteome-wide protein quantification. *Nat*
529 *Biotechnol*. 2008;26: 1367–72.
- 530 40. Sloothaak J, Odoni DI, de Graaff LH, Martins Dos Santos VAP, Schaap PJ, Tamayo-
531 Ramos JA. *Aspergillus niger* membrane-associated proteome analysis for the
532 identification of glucose transporters. *Biotechnol Biofuels*. 2015;8: 150.
- 533 41. Vizcaíno JA, Csordas A, Del-Toro N, Dianes JA, Griss J, Lavidas I, et al. 2016 update
534 of the PRIDE database and its related tools. *Nucleic Acids Res*. Oxford University
535 Press; 2016;44: D447–D456.
- 536 42. Claudel-Renard C, Chevalet C, Faraut T, Kahn D. Enzyme-specific profiles for genome
537 annotation: PRIAM. *Nucleic Acids Res*. 2003;31: 6633–9.
- 538 43. Kanehisa M, Goto S. KEGG: kyoto encyclopedia of genes and genomes. *Nucleic Acids*
539 *Res*. 2000;28: 27–30.
- 540 44. Kanehisa M, Sato Y, Kawashima M, Furumichi M, Tanabe M. KEGG as a reference
541 resource for gene and protein annotation. *Nucleic Acids Res*. 2015;44: D457–62.
- 542 45. R Core T. R: A language and environment for statistical computing. R Foundation for
543 Statistical Computing, Vienna, Austria.; 2014.
- 544 46. Cao N, Du J, Gong CS, Tsao GT. Simultaneous Production and Recovery of Fumaric
545 Acid from Immobilized *Rhizopus oryzae* with a Rotary Biofilm Contactor and an
546 Adsorption Column. *Appl Environ Microbiol*. 1996;62.
- 547 47. Lin MS, Wang HH. Anaerobic growth and oxygen toxicity of *Rhizopus cultures*
548 isolated from starters made by solid state fermentation. *Zhonghua Min Guo Wei Sheng*
549 *Wu Ji Mian Yi Xue Za Zhi*. 1991;24: 229–39.
- 550 48. Weusthuis RA, Visser W, Pronk JT, Scheffers WA, van Dijken JP. Effects of oxygen
551 limitation on sugar metabolism in yeasts: a continuous-culture study of the Kluver
552 effect. *Microbiology*. 1994;140 Pt 4: 703–15.
- 553 49. Gu S, Xu Q, Huang H, Li S. Alternative respiration and fumaric acid production of
554 *Rhizopus oryzae*. *Appl Microbiol Biotechnol*. 2014;98: 5145–52.
- 555 50. Vanlerberghe GC. Alternative oxidase: a mitochondrial respiratory pathway to
556 maintain metabolic and signaling homeostasis during abiotic and biotic stress in plants.
557 *Int J Mol Sci*. Multidisciplinary Digital Publishing Institute; 2013;14: 6805–47.
- 558 51. Johnson MA, Vidoni S, Durigon R, Pearce SF, Rorbach J, He J, et al. Amino acid
559 starvation has opposite effects on mitochondrial and cytosolic protein synthesis. *PLoS*
560 *One*. Public Library of Science; 2014;9: e93597.